Article

Numerical Study on Mixed Convection Flow and Energy Transfer in an Inclined Channel Cavity: Effect of Baffle Size

Sivanandam Sivasankaran [1],*[ID] and Kandasamy Janagi [2]

1   Department of Mathematics, King Abdulaziz University, Jeddah 21589, Saudi Arabia
2   Department of Mathematics, KPR Institute of Engineering and Technology, Coimbatore 641048, India; janu149.kpr@gmail.com
*   Correspondence: sd.siva@yahoo.com or smsivanandam@kau.edu.sa

Abstract: The objective of the current numerical study is to explore the combined natural and forced convection and energy transport in a channel with an open cavity. An adiabatic baffle of finite length is attached to the top wall. The sinusoidal heating is implemented on the lower horizontal wall of the open cavity. The other areas of the channel cavity are treated as adiabatic. The governing equations are solved by the control volume technique for various values of relevant factors. The drag force, bulk temperature and average Nusselt number are computed. It is recognised that recirculating eddies beside the baffle become weak or disappear upon increasing the inclination angle of the channel/cavity. The average thermal energy transportation reduces steadily until the $Ri = 1$ and then it rises for all inclination angles and lengths of the baffle.

Keywords: cavity channel; mixed convection; baffle; inclination

1. Introduction

Over the decades, the research on mixed convective stream and thermal energy transference in channel cavities are of fundamental interest in applied science research because of its applications in several fields [1–10]. Manca et al. [11] discovered the influence of the location of a hot wall on the combined convective flow of an open cavity that exists in a channel. Leong et al. [12] performed the study on combined convection in an open cavity inside a horizontal flat channel. Rahman et al. [13] numerically explored the magneto-convection in a flat horizontal channel cavity with bottom heating. Rahman et al. [14] numerically considered the mixed convection in a channel with an open cavity with a fully or partly heated left sidewall. They discovered that the energy transfer enhancement was recognised at higher values of Ra with a partial heater. Sharma et al. [15] considered a channel in a grooved manner to examine the combined convection with a baffle attached on the top-side of the channel. They observed a remarkable rise of heat transport in the occurrence of the partition at a mixed convective range.

The influence of several thermal border conditions on convective energy transport was observed by several studies due to applications of such boundary conditions in various fields. Janagi et al. [16] explored the convective energy transport of water in a square container with sinusoidal thermal heating. Cheong et al. [17] numerically explored the buoyant convection in a wavy walled box with heat generation and sinusoidal heating effects. The impact of heating the sidewalls sinusoidally in the study on convective dynamism was found in [18,19]. Li et al. [20] analysed heat transfer characteristics of nanoliquids in an enclosed area with variable thermal properties by connected and unconnected heaters. Bhardwaj et al. [21] numerically analysed the convective thermal energy transport and entropy generation in a wavy porous enclosed box with uneven heating.

The influence of geometry inclination is a key factor on buoyant convective flow and energy transport systems. The influence due to the inclination angle contributes a significant part in the refrigeration of electronic equipment, particularly the interior of modern gadgets,

computers and laptops. This type of equipment requires effort at diverse inclination angles in different environmental conditions. Sivasankaran et al. [22] explored the influence of the direction of a wall in motion on convective energy transport in an inclined box encompassing sinusoidal thermal conditions at the wall. Cheong et al. [23] exposed the effect of an aspect ratio on an inclined box with sinusoidal temperature conditions on the wall. Sivakumar and Sivasankaran [24] examined the effect of inclination on a convective stream in an enclosed box with different heating constraints. Hadidi et al. [25] examined the significance of the inclination angle on a double-diffusive convective current in a flat dual-layered porous container.

The baffle or partition inside the channels and cavities plays an important role in convective flow under various situations [26–29]. Mahapatra et al. [30] discovered the opposite combined convective stream in a partitioned box with two partitions attached in the bottom and top walls. Ilis et al. [31] numerically explored the ceiling-mounted baffle on buoyant convection in a box. Khatamifar et al. [32] inspected conjugate convective current in a box separated by a divider. They examined the effect of the divider thickness and thermal conductivity under various parameters.

No work is described in the literature that discovers the effect of the inclination angle and partition length on convective transfer in a channel cavity at an inclined position. This problem has many applications in electronic equipment cooling and the cooling of thermal systems. Therefore, the current problem explores the impact of inclination angle and adiabatic partition length on convective energy transport in a channel with an open cavity.

2. Mathematical Methods

Consider the 2-dimensional, incompressible, steady, laminar flow in a passage (channel) with an open cavity of width $L/2$ and length L, as displayed in Figure 1. The lower horizontal wall of the open cavity holds a higher temperature than the temperature of the flowing liquid. The channel cavity is inclined with the horizontal plane at an angle (ϕ). An adiabatic baffle of length L_B is attached at the top wall and its length varies inside the cavity. The gravitational force acts downwards.
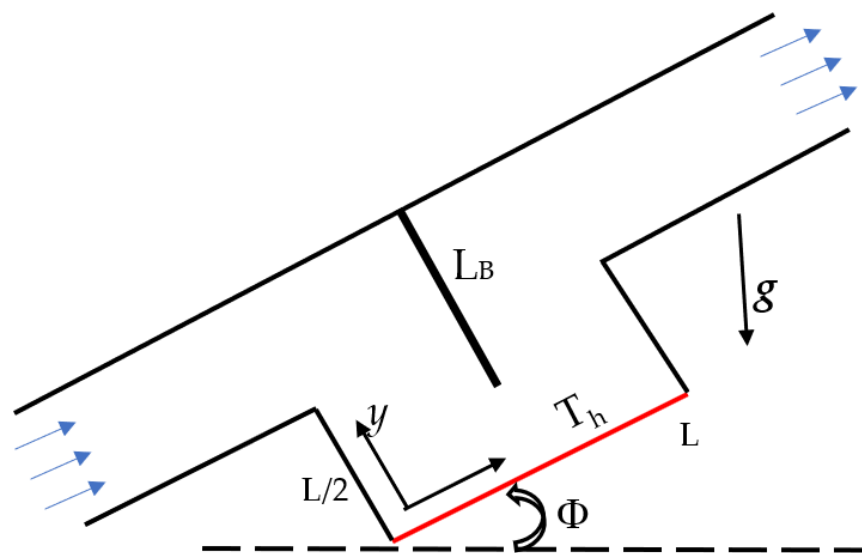

Figure 1. Physical model.

The leading equations for the existing model with Boussinesq approximations are [11,12,23,24]:

$$\frac{\partial u}{\partial x} + \frac{\partial v}{\partial y} = 0 \qquad (1)$$

$$u\frac{\partial u}{\partial x} + v\frac{\partial u}{\partial y} = -\frac{1}{\rho_0}\frac{\partial p}{\partial x} + v\left(\nabla^2 u\right) + g\beta(\theta - \theta_c)Sin(\Phi) \qquad (2)$$

$$u\frac{\partial v}{\partial x} + v\frac{\partial v}{\partial y} = -\frac{1}{\rho_0}\frac{\partial p}{\partial y} + v\left(\nabla^2 v\right) + g\beta(\theta - \theta_c)Cos(\Phi) \qquad (3)$$

$$u\frac{\partial T}{\partial x} + v\frac{\partial T}{\partial y} = \alpha\left(\nabla^2 T\right) \qquad (4)$$

where (u, v) are velocities, g is gravitational acceleration, p represents pressure, T represents temperature, ρ_0 is density, α is heat diffusivity, β is thermal expansion coefficient, and v is kinematic viscosity, respectively.

The initial and end settings are [11,12]

$$
\begin{aligned}
\text{Inlet}: \ & v = 0, u = U_0; \ T = 0 \\
\text{Outlet}: \ & v = 0, \ \frac{\partial u}{\partial x} = 0; \ \frac{\partial T}{\partial x} = 0, \ p = 0 \\
\text{Bottom}: \ & v = 0, u = 0; \ T = T_h(x) = Sin\left(\frac{\pi x}{L}\right)(T_h - T_c) + T_c \\
\text{Other sides \& baffle}: \ & v = 0, u = 0; \ \frac{\partial T}{\partial n} = 0
\end{aligned}
\qquad (5)
$$

where "n" is normal to the surface. The non-dimensionalised equations are obtained using the measures $(X, Y) = (x, y)/L$, $(U, V) = (u, v)/U_0$, $P = p/\left(\rho U_0^2\right)$, $\theta = (T - T_c)/(T_h - T_c)$. The following are the dimensionless system of equations [11,12,23]:

$$\frac{\partial U}{\partial X} + \frac{\partial V}{\partial Y} = 0 \qquad (6)$$

$$U\frac{\partial U}{\partial X} + V\frac{\partial U}{\partial Y} = -\frac{\partial P}{\partial X} + \frac{1}{Re}\left(\frac{\partial^2 U}{\partial X^2} + \frac{\partial^2 U}{\partial Y^2}\right) + \frac{Gr}{Re^2}\theta\,Sin(\Phi) \qquad (7)$$

$$U\frac{\partial V}{\partial X} + V\frac{\partial V}{\partial Y} = -\frac{\partial P}{\partial Y} + \frac{1}{Re}\left(\frac{\partial^2 V}{\partial X^2} + \frac{\partial^2 V}{\partial Y^2}\right) + \frac{Gr}{Re^2}\theta\,Cos(\Phi) \qquad (8)$$

$$U\frac{\partial \theta}{\partial X} + V\frac{\partial \theta}{\partial Y} = \frac{1}{RePr}\left(\frac{\partial^2 \theta}{\partial X^2} + \frac{\partial^2 \theta}{\partial Y^2}\right) \qquad (9)$$

The non-dimensional parameters are, $Gr = \frac{g\beta(\theta_h - \theta_c)L^3}{v^2}$, Grashof number, $Re = \frac{U_0 L}{v}$, Reynolds number, $Pr = \frac{v}{\alpha}$, Prandtl number, and $Ri = \frac{Gr}{Re^2}$, Richardson number. The stream function is constructed by using $U = \Psi_Y$ and $V = -\Psi_X$. The non-dimensional settings at borders for the current problem are [11,12]:

$$
\begin{aligned}
\text{Inlet}: \ & U = 1, \ V = 0, \ \theta = 0 \\
\text{Outlet}: \ & \frac{\partial U}{\partial X} = 0, \ V = 0, \ \frac{\partial \theta}{\partial X} = 0, \ P = 0 \\
\text{Lower wall}: \ & U = 0, \ V = 0, \ \theta = \theta_h(X) = Sin(\pi X) \\
\text{Other walls \& baffle}: \ & U = 0, \ V = 0, \ \frac{\partial \theta}{\partial n} = 0
\end{aligned}
\qquad (10)
$$

Here, the physical measures of the current analysis are constructed. The non-dimensionally average Nusselt number of the hot surface is computed as $Nu = -\int_0^1 \frac{\partial \theta}{\partial Y}dX$, the drag force is derived as, $D = -\int_0^1 \frac{\partial U}{\partial Y}dX$ and the average heat value of the liquid is defined as $\theta_{avg} = \int \theta d\overline{V}/\overline{V}$, where $\overline{V}$ is the volume of the domain.

3. Numerical Method

The resultant mathematical models are evaluated numerically by using the finite volume method. The discretised algebraic systems acquired here are solved iteratively. To decide the appropriate size of the grid for the current work, a grid independence examination is executed with $Ri = 1$. The several sizes of meshes (41 × 41 to 201 × 201) are taken for this independence test. We did all the calculations with a grid size of 161 × 161 here. The numerical simulations are terminated after reaching the convergence of order,

10^{-6}. The Trapezoidal rule is used to compute the physical quantities of transport rate along the surface. The more detailed numerical procedure is found in [18,19].

4. Results and Discussion

The mathematical calculations are equipped for various angles of inclination of the channel cavity and the length of baffle with several values of the Richardson number $(0.01 \leq Ri \leq 100)$. The value of the Grashof number is fixed as 10^5, and the Reynolds numbers are chosen as $31.6 \leq Re \leq 3162$. The Prandtl number value used is 0.71. The length of the baffle is used as $L_B = 0, 0.25, 0.5, 0.75$. The inclination angle is chosen as $0 \leq \phi \leq 90$.

Figure 2 shows the flow field for various inclination angles and Richardson numbers with a length of the baffle, $L_B = 0.5$. It is evidently seen that the combined convection factor (Ri) impacts greatly on the stream arrangement. The re-circulation eddies form beside the partition in the forced convective region $(Ri = 0.01)$ for every value of inclination angle. Such behaviour does not appear in mixed and buoyant convective regimes for higher inclination angles. The eddy occupies the majority of the open cavity when $Ri \leq 1$ in the absence of inclination. When increasing the inclination angle, the eddy inside the cavity shrinks in its size and the core region moves to the right end of the cavity at $Ri = 0.01$. At $Ri = 1$, the eddy inside the cavity becomes very weak and moves towards the left side of the cavity. However, there is no recirculating eddy inside the cavity in the free convection regime. There exists a recirculating eddy at the right side of the baffle in a free convection regime for inclination angles. Figure 3 portrays the thermal distribution inside the channel cavity for various inclination angles and Richardson numbers with a length of the baffle, $L_B = 0.5$. The vigorous thermal boundary layers formed along the lower-heated wall. It shows that the convective type of energy transference is controlled in all the cases considered here. There is no temperature change in the channel portion in the mixed convective regime. However, significant changes in temperature are observed inside the channel area with the free convective regime.

Figure 4 demonstrates the impact of baffle length on the convective stream inside the channel cavity for several tilting angles with $Ri = 1$. The strong recirculating eddies are formed within the cavity area in the nonappearance of a partition without inclination. The strong recirculating eddies disappeared when the channel cavity is subjected to an incline. When the baffle exists, small recirculating eddies are created on both sides of the baffle. However, those recirculating eddies become weak or disappear when increasing the inclination angle of the system. Figure 5 shows the corresponding thermal distribution for the pertinent parameters in Figure 4. The temperature gradient is high inside the cavity area than that of the channel area. The stream is not vigorously flowing inside the open cavity in the absence of an adiabatic partition and heat transmission is feeble from the source. The baffle aids the stream to travel along the cavity and disturbs the heat energy conveyance. The energy transfer enhances on increasing the size of the partition because the stream is forced inside the open cavity by the existence of the baffle and results in a higher energy transference inside the open cavity.

Figure 6a–d establish the drag force for diverse values of Ri, inclination angle and size of the partition. The drag force steadily rises with Richardson number for all inclination angles when $L_B \leq 0.25$. The drag force behaves nonlinearly with the Ri number for all inclination angles when $L_B = 0.75$. It reduces sharply until $Ri = 1$ and then it grows when increasing the value of Ri for all inclinations. However, it diminishes sharply until $Ri = 10$ for the non-inclined case. The variation in drag force among the inclination angle is not significant in the forced convective regime when $L_B \leq 0.5$. Figure 7a–d portray the average temperature for various values of Ri, inclination and sizes of the baffle. The average temperature performs non-linearly with the Ri number for all inclined cases when $L_B \leq 0.5$. The average temperature enhances with the Richardson number for the case of $L_B = 0.75$. However, there is no significant variation in the average temperature among the inclinations for $L_B = 0.75$. The average temperature is high at $Ri = 100$.
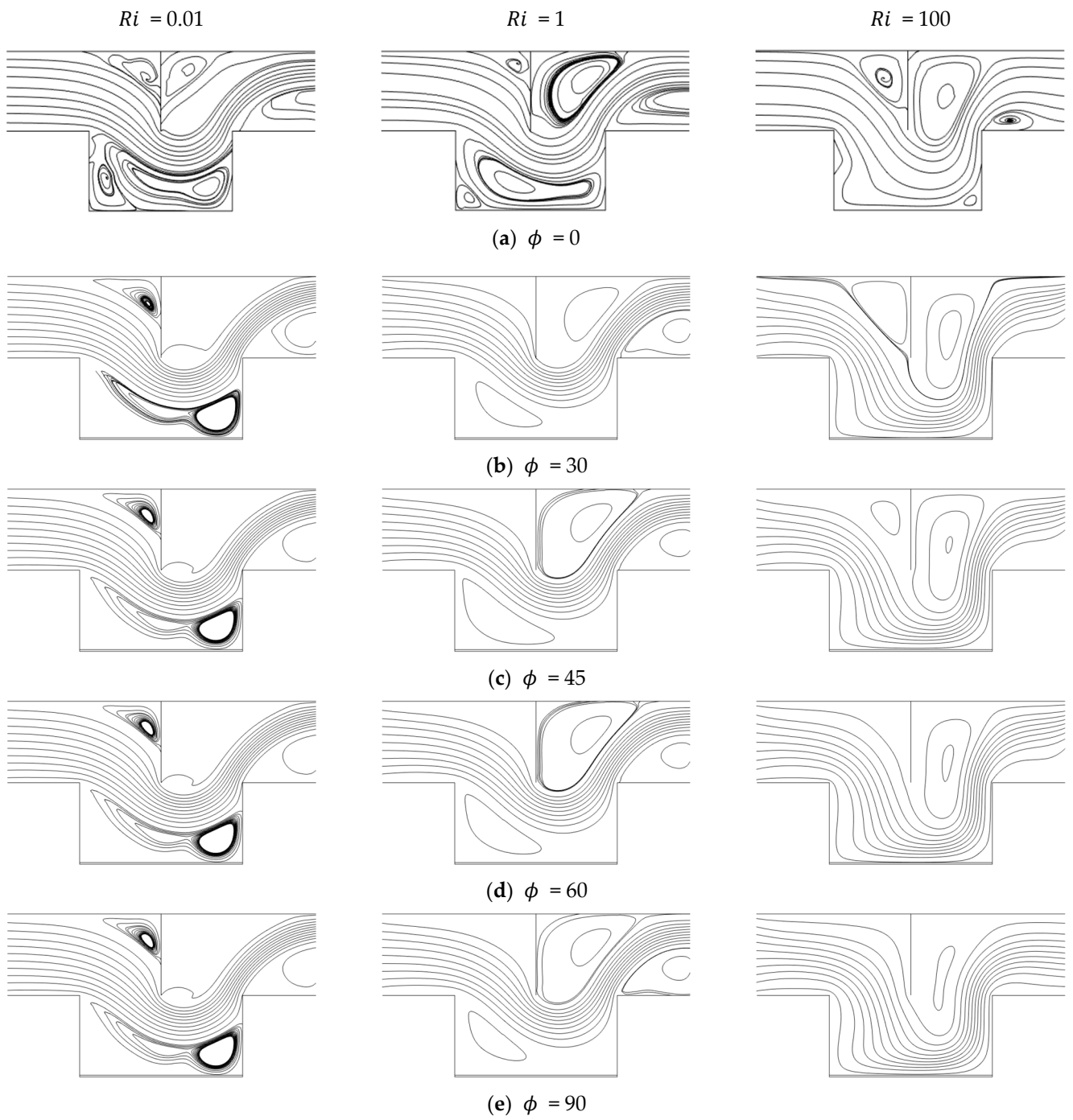
Ri = 0.01　　　　　Ri = 1　　　　　Ri = 100

(a) ϕ = 0

(b) ϕ = 30

(c) ϕ = 45

(d) ϕ = 60

(e) ϕ = 90

Figure 2. Streamlines for various values of *Ri* and inclination angles with L_B = 0.5.
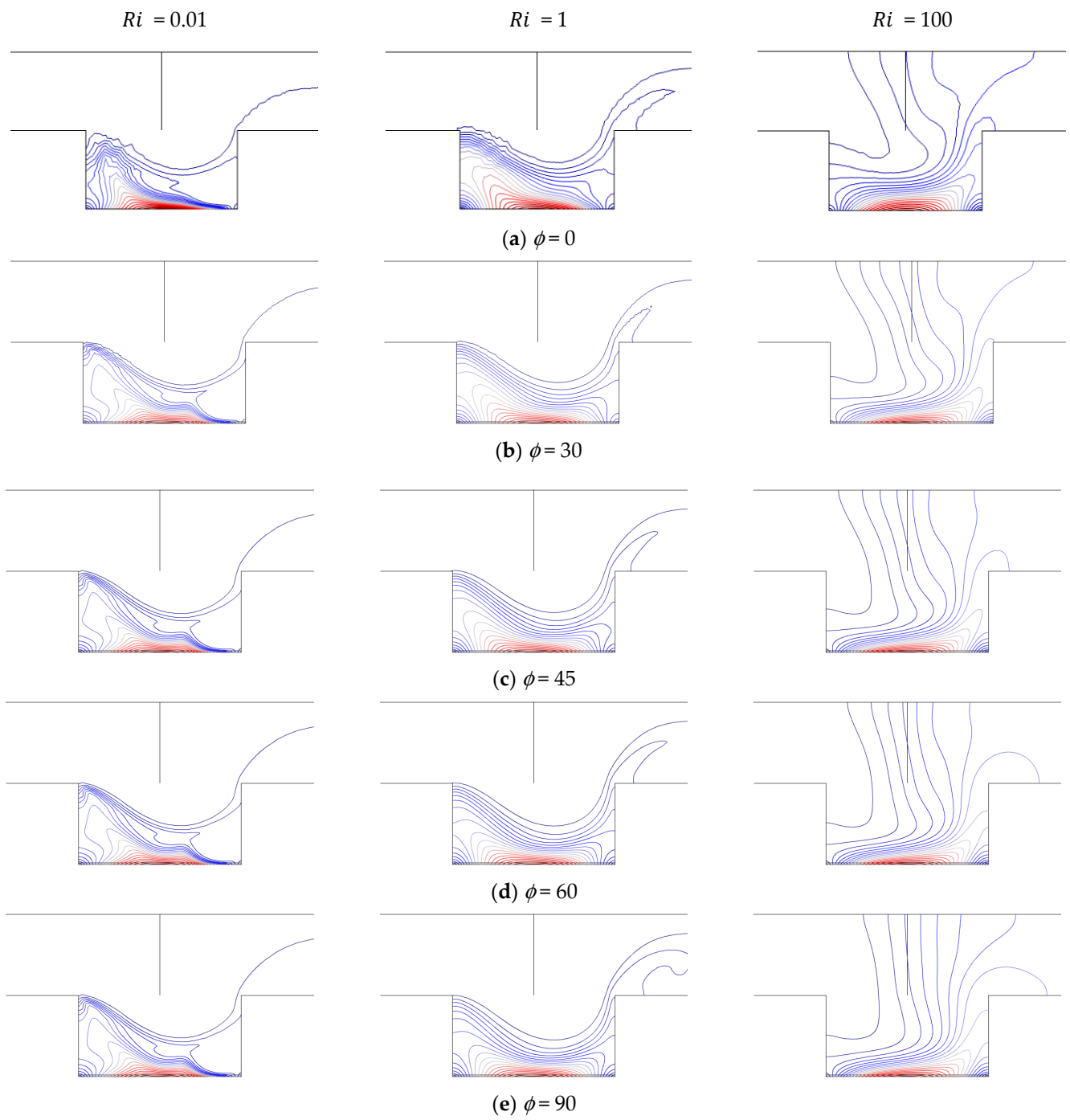
Figure 3. Isotherms for various values of *Ri* and inclination angles with $L_B = 0.5$.
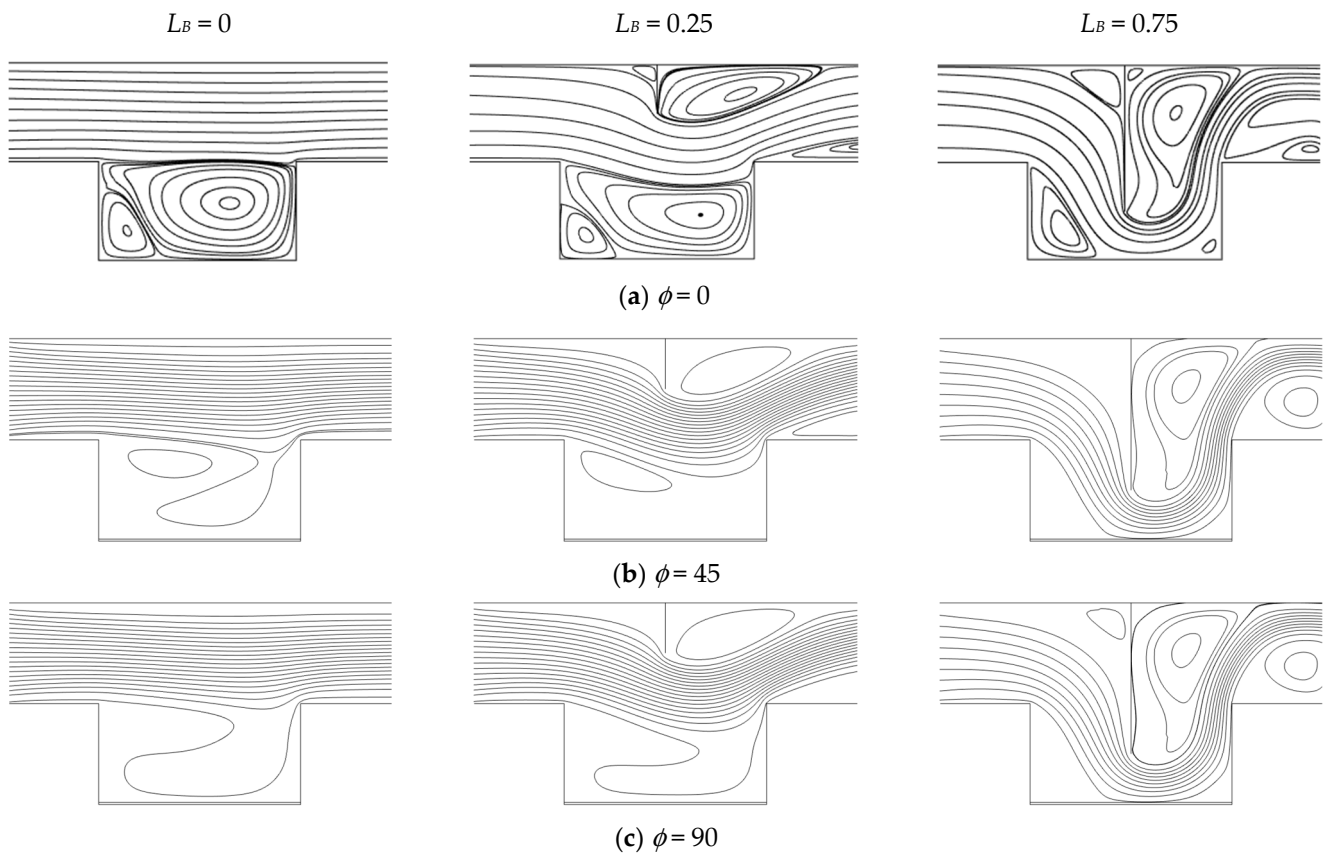
(**a**) $\phi = 0$

(**b**) $\phi = 45$

(**c**) $\phi = 90$

Figure 4. Streamlines for various L_B and ϕ values with $Ri = 1.0$.

$L_B = 0$ $L_B = 0.25$ $L_B = 0.75$

(**a**) $\phi = 0$

(**b**) $\phi = 45$

(**c**) $\phi = 90$
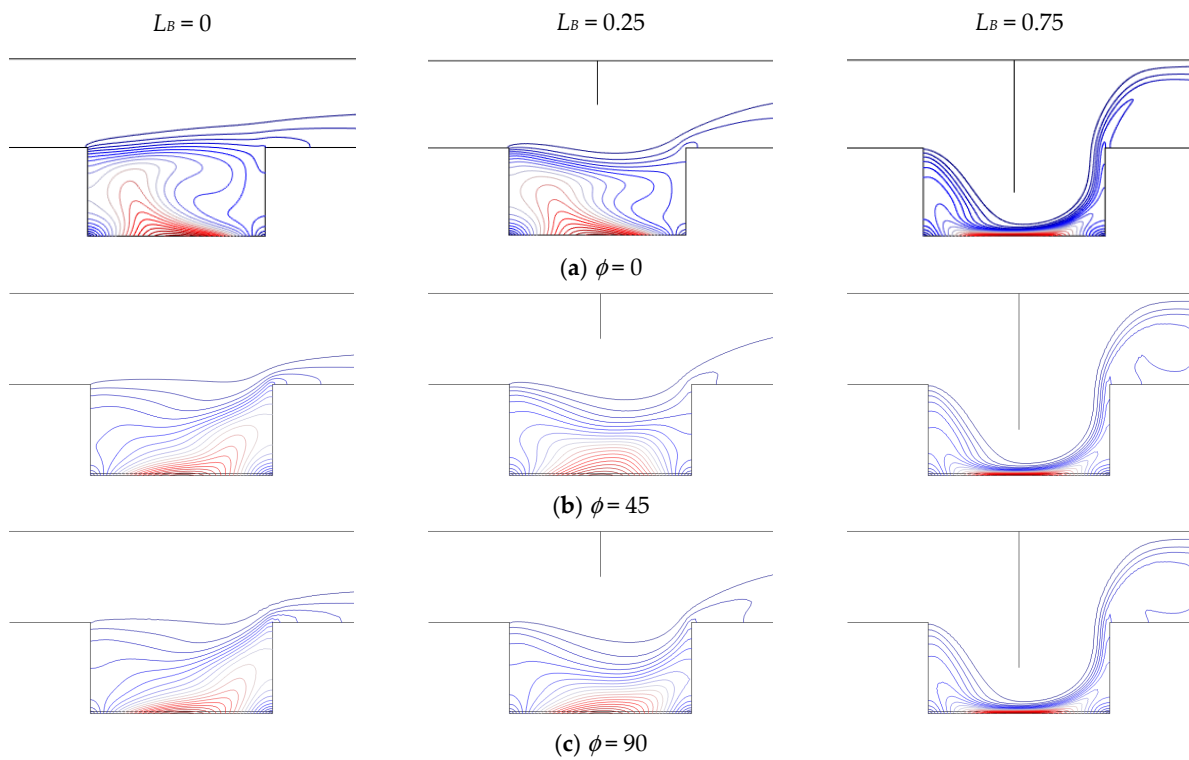
Figure 5. Isotherms for various L_B and ϕ values with $Ri = 1.0$.
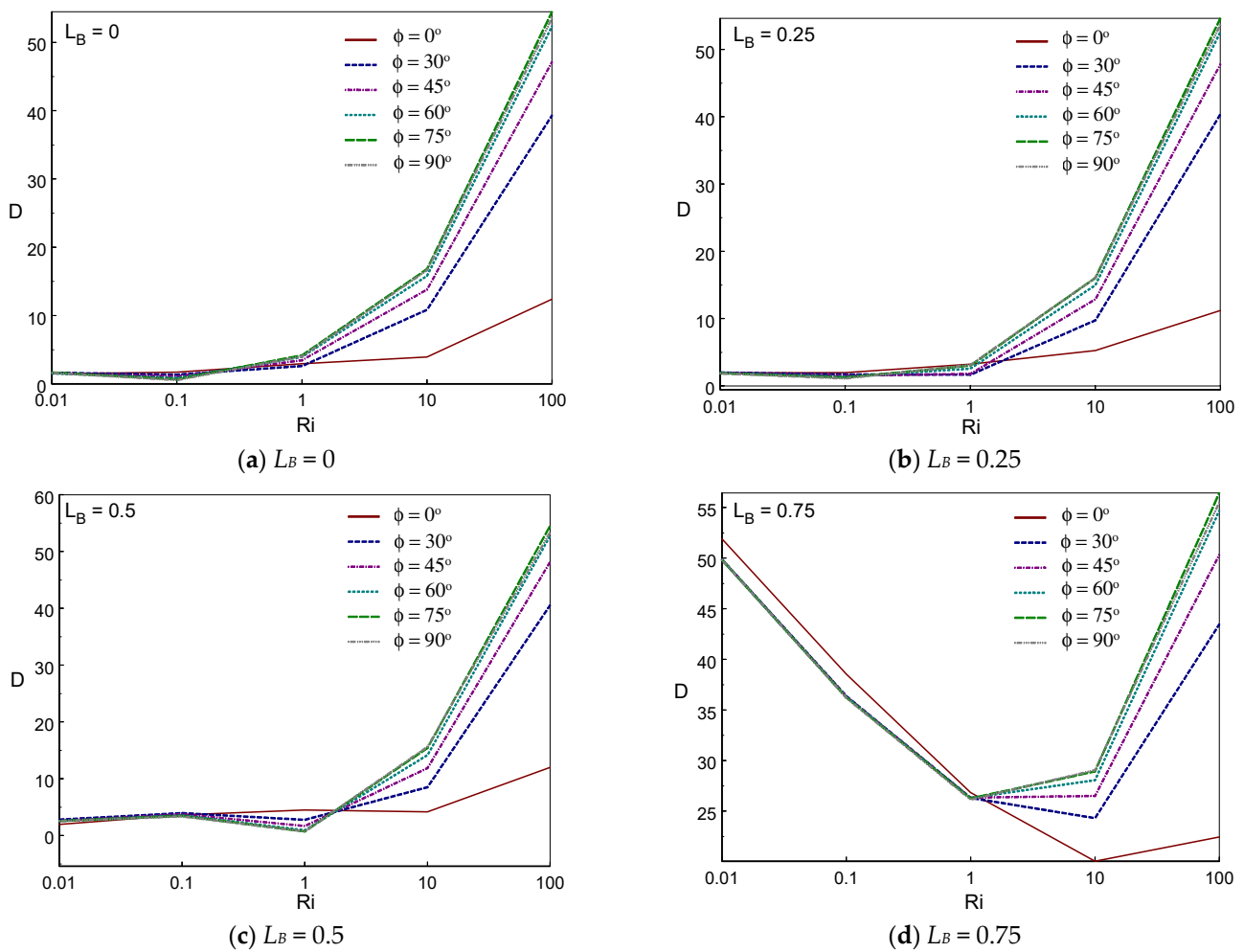
Figure 6. Drag force vs. *Ri* for variations of L_B and ϕ values.

Figure 8a–d demonstrate the local Nusselt number for numerous inclination angles of the channel cavity, diverse *Ri* and two cases of the length of the baffle. The shapes of local Nu evidently indicate the immediate influence of an imposed sinusoidal thermal condition on the lower hot wall. The highest local thermal energy transference is attained near the middle of the bottom wall with *Ri* = 100 for inclinations. However, the highest local heat energy transport occurs around *Y* = 3/4 with *Ri* = 0.01. In addition, it is understood that the local thermal energy transport is enhanced slightly when increasing the inclination of the channel cavity for all values of *Ri*. The thermal energy transport is more pronounced with the occurrence of the baffle in the forced convective regime more than that of the buoyant convection regime. Figure 9a–d indicate the average energy transmission rate versus the Richardson number for numerous values of inclination angle and lengths of the baffle. The mean value of thermal energy transference reduces steadily till *Ri* = 1 and then it rises for all inclination angles and lengths of the baffle. However, the average Nusselt number declines until *Ri* = 10 for the non-inclined case. It is witnessed that increments in the baffle size increase the average thermal dynamism. When comparing the inclination angles, no constant angle provides a higher heat transport inside the channel cavity.
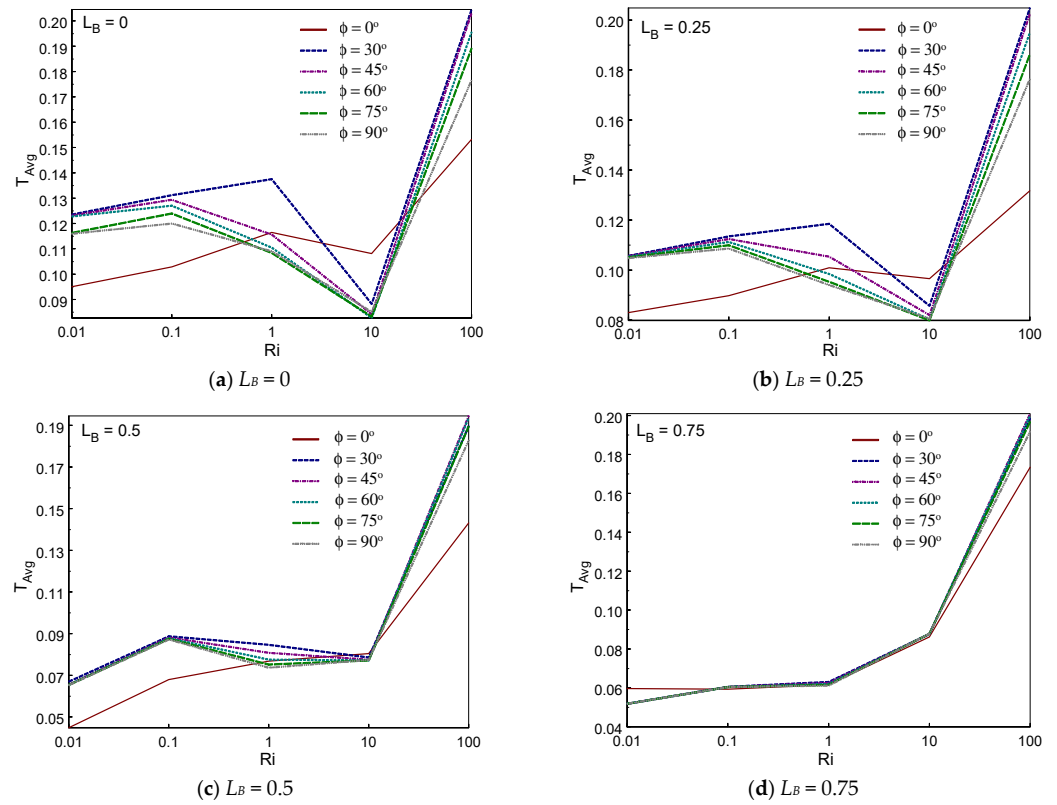
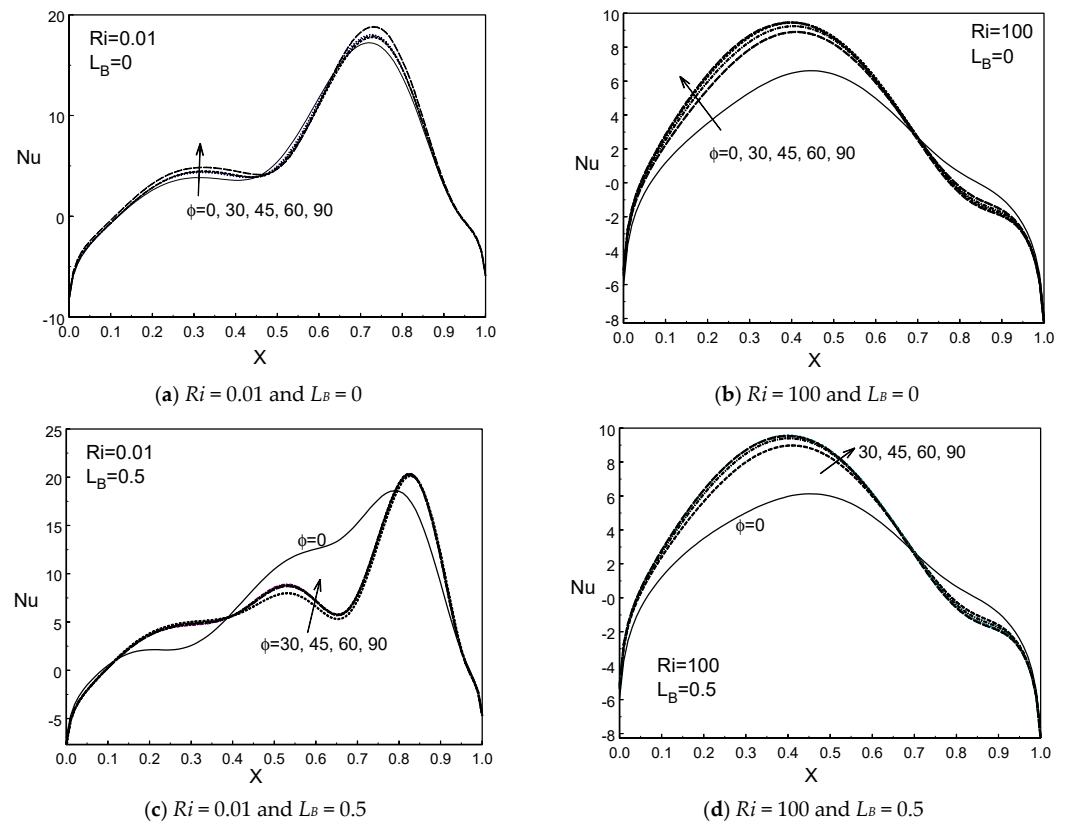**Figure 7.** Average temperature vs. *Ri* for variations of L_B and ϕ values.

Figure 8. Local Nusselt number for various inclination angles, L_B and *Ri*.
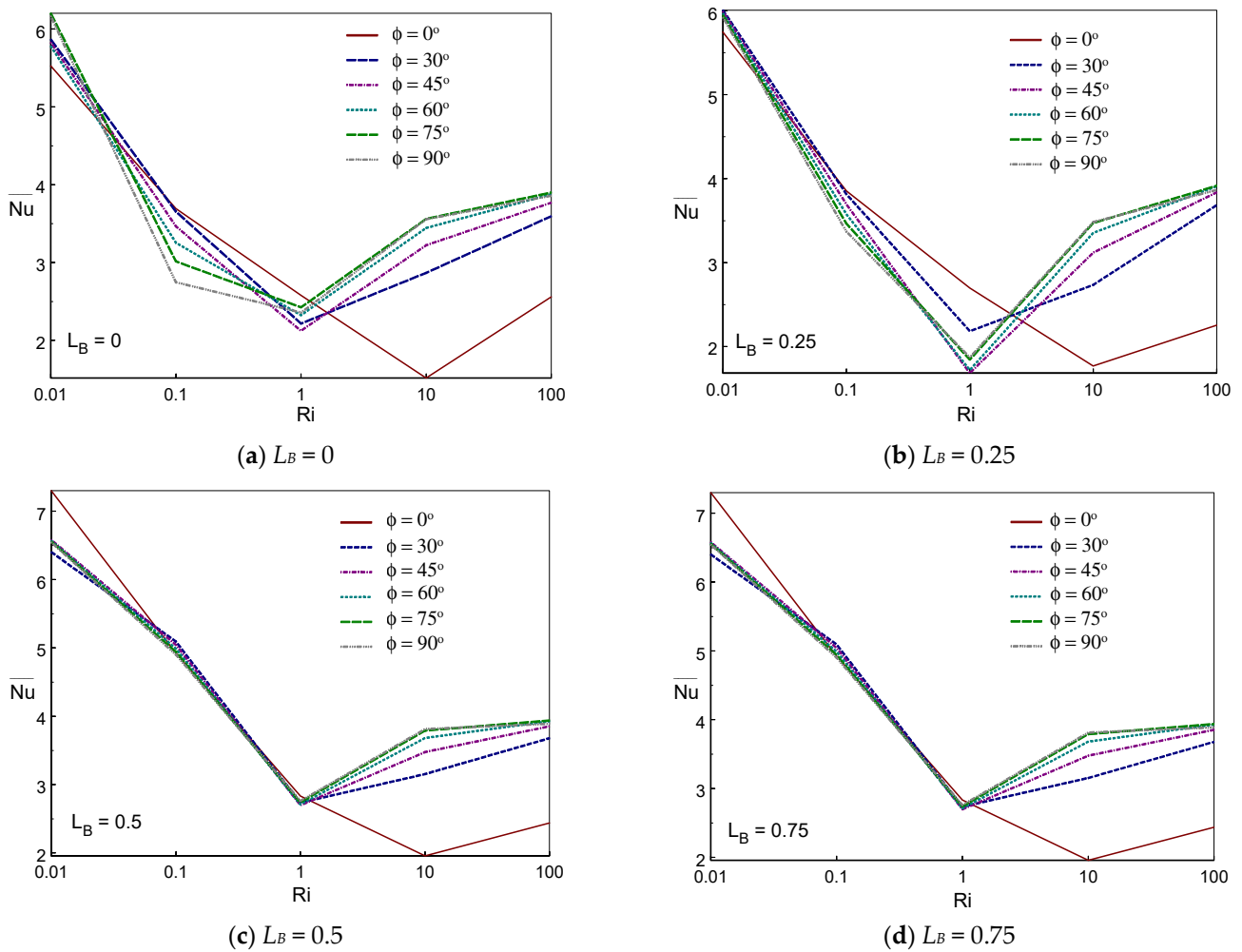
Figure 9. Average *Nu* vs. *Ri* for variations of L_B and ϕ.

Figure 10a–c portray the increment in the average Nu between the presence of a baffle and the absence of a baffle inside the channel cavity for distinct values of the angle of inclination and *Ri*. Figure 10a demonstrates the comparison of the average Nusselt number between $L_B = 0$ and $L_B = 0.25$. The increment in heat transport is observed in the occurrence of a baffle in the forced convective regime for all tilting angles except at a *Ri* = 0.01 and $\phi = 90°$. The mixed convection regime provides a decrement in energy transportation for all inclined channel cavity cases. Figure 10b clearly shows that an increment in thermal energy transportation is observed in all cases of *Ri* and inclination angles, except Ri = 100 and $\phi = 0°$. The energy transfer increases by around 80% at *Ri* = 0.1 and $\phi = 90°$ with $L_B = 0.25$ compared to the absence of a baffle. Figure 10c undoubtedly indicates that there is no decrement in energy transfer with $L_B = 0.75$ compared with the absence of a baffle. The highest amount of heat transport is about 450% with $L_B = 0.75$ at *Ri* = 0.1 and $\phi = 90°$. Further, it is concluded from these figures that the increment of energy transportation grows when increasing the size of the baffle.
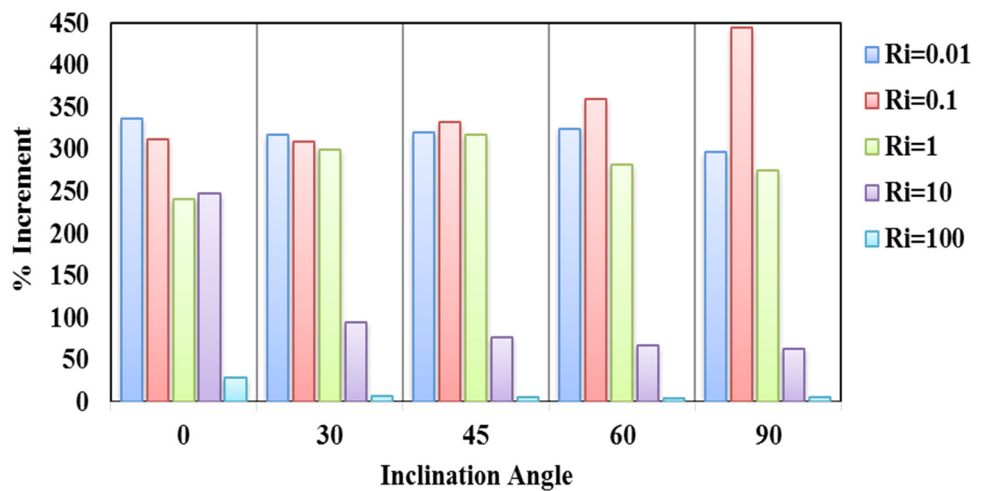
(**a**) $L_B = 0.25$

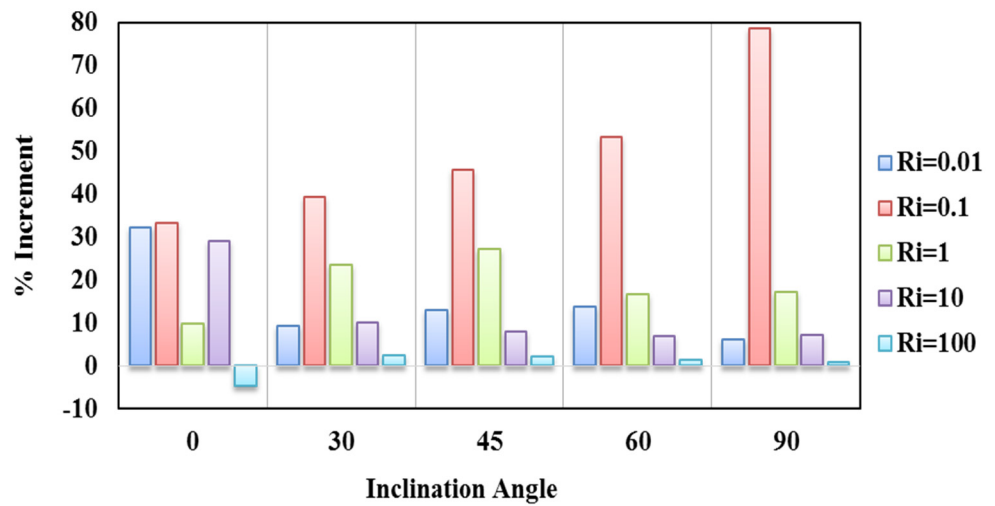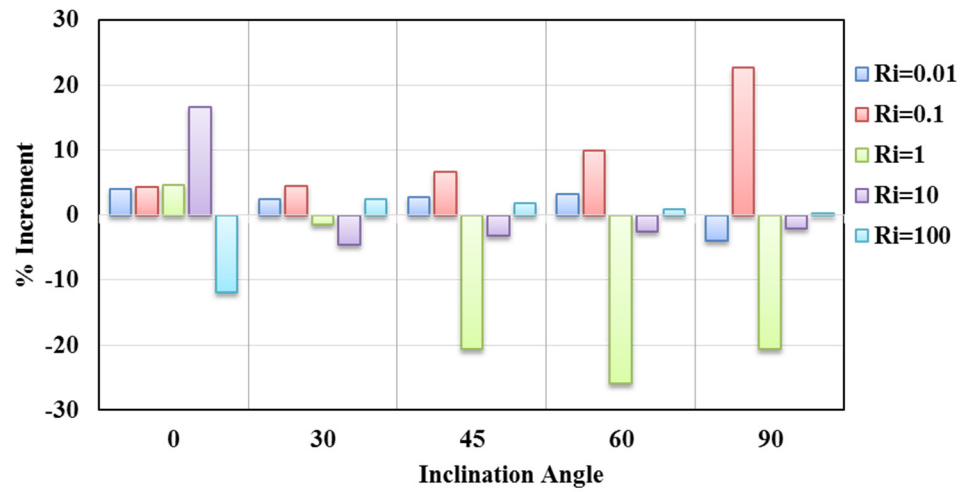(**b**) $L_B = 0.5$

(**c**) $L_B = 0.75$

Figure 10. Comparison of the average Nu for different lengths of baffle and various inclination angles and Richardson numbers with $L_B = 0$.

5. Conclusions

The influences of the inclination angle and the length of the adiabatic baffle on convective motion and thermal energy transportation in a passage with an open cavity are inspected numerically. The bottom wall of the channel cavity is exposed to sinusoidal heating. The results are scrutinised for numerous arrangements of baffle size, inclination angle and *Ri*. The following conclusions are drawn:

○ The recirculating eddies beside the baffle become weak or disappear when increasing the inclination angle of the channel cavity.

○ The energy transfer enriches when enhancing the baffle size since the stream further induces the inner part of the cavity with the existence of the partition, resulting in an enormous energy transference within the cavity.

○ The average thermal energy transportation reduces steadily until the *Ri* = 1 and then it rises for all inclination angles and lengths of the baffle. When comparing the inclination angles, no constant angle provides a higher heat transport inside the channel cavity.

○ The increment of energy transference enhances when increasing the size of the baffle. The highest quantity of heat transport is found to be about 450% with the occurrence of a baffle.

Author Contributions: Conceptualization, S.S.; methodology, S.S.; software, S.S.; validation, S.S.; formal analysis, S.S.; investigation, S.S.; writing—original draft preparation, S.S. and K.J.; writing—review and editing, S.S. and K.J.; visualization, S.S.; supervision, S.S. All authors have read and agreed to the published version of the manuscript.

References

1. You, X.; Li, S. Fully Developed Opposing Mixed Convection Flow in the Inclined Channel Filled with a Hybrid Nanofluid. *Nanomaterials* **2021**, *11*, 1107. [CrossRef] [PubMed]
2. Borrelli, A.; Giantesio, G.; Patria, M.C. Magnetohydrodynamic Flow of a Bingham Fluid in a Vertical Channel: Mixed Convection. *Fluids* **2021**, *6*, 154. [CrossRef]
3. Khan, S.I.U.; Alzahrani, E.; Khan, U.; Zeb, N.; Zeb, A. On Mixed Convection Squeezing Flow of Nanofluids. *Energies* **2020**, *13*, 3138. [CrossRef]
4. Mohamed, A.B.; Hdidi, W.; Tlili, I. Evaporation of Water/Alumina Nanofluid Film by Mixed Convection Inside Heated Vertical Channel. *Appl. Sci.* **2020**, *10*, 2380. [CrossRef]
5. Armaghani, T.; Ismael, M.A.; Chamkha, A.J.; Pop, I. Mixed Convection and Entropy Generation of an Ag-Water Nanofluid in an Inclined L-Shaped Channel. *Energies* **2019**, *12*, 1150. [CrossRef]
6. Ozgen, F.; Varol, Y. Numerical Study of Mixed Convection in a Channel Filled with a Porous Medium. *Appl. Sci.* **2019**, *9*, 211. [CrossRef]
7. Carozza, A. Numerical Study on Mixed Convection in Ventilated Cavities with Different Aspect Ratios. *Fluids* **2018**, *3*, 11. [CrossRef]
8. Sivasankaran, S.; Sivakumar, V.; Hussein, A.K. Numerical study on mixed convection in a lid-driven cavity with discrete heating. *Int. Comm. Heat Mass Transf.* **2013**, *46*, 112–125. [CrossRef]
9. Roy, M.; Roy, S.; Basak, T. Role of various moving walls on energy transfer rates via heat flow visualization during mixed convection in square cavities. *Energy* **2015**, *82*, 1–22. [CrossRef]
10. Sivasankaran, S.; Niranjan, H.; Bhuvaneswari, M. Chemical reaction, radiation and slip effects on MHD mixed convection stagnation-point flow in a porous medium with convective boundary condition. *Int. J. Numer. Methods Heat Fluid Flow* **2017**, *27*, 454–470. [CrossRef]
11. Manca, O.; Nardini, S.; Khanafer, K.; Vafai, K. Effect of heated wall position on mixed convection in a channel with an open cavity. *Numer. Heat Transfer A* **2003**, *43*, 259–282. [CrossRef]
12. Leong, J.C.; Brown, N.M.; Lai, F.C. Mixed convection from an open cavity in a horizontal channel. *Int. Comm. Heat Mass Transf.* **2005**, *32*, 583–592. [CrossRef]
13. Rahman, M.M.; Öztop, H.F.; Saidur, R.; Mekhilef, S.; Al-Salem, K. Finite element solution of MHD mixed convection in a channel with a fully or partially heated cavity. *Comput. Fluids* **2013**, *79*, 53–64. [CrossRef]
14. Rahman, M.M.; Parvin, S.; Saidur, R.; Rahim, N.A. Magneto-hydrodynamic mixed convection in a horizontal channel with an open cavity. *Int. Comm. Heat Mass Transf.* **2011**, *38*, 184–193. [CrossRef]

15. Sharma, A.K.; Mahapatra, P.S.; Manna, N.K.; Ghosh, K. Mixed convection heat transfer in a grooved channel in the presence of a baffle. *Numer. Heat Transf. Part A* **2015**, *67*, 1097–1118. [CrossRef]

16. Janagi, K.; Sivasankaran, S.; Bhuvaneswari, M.; Eswaramurthi, M. Numerical study on free convection of cold water in a square porous cavity with sinusoidal wall temperature. *Int. J. Numer. Methods Heat Fluid Flow* **2017**, *27*, 1000–1014. [CrossRef]

17. Cheong, H.T.; Sivasankaran, S.; Bhuvaneswari, M. Natural convection in a wavy porous cavity with sinusoidal heating and internal heat generation. *Int. J. Numer. Methods Heat Fluid Flow* **2017**, *27*, 287–309. [CrossRef]

18. Sivasankaran, S.; Bhuvaneswari, M. Natural convection in a porous cavity with sinusoidal heating on both sidewalls. *Numeri. Heat Transf. A* **2013**, *63*, 14–30. [CrossRef]

19. Bhuvaneswari, M.; Sivasankaran, S.; Kim, Y.J. Magneto-convection in an enclosure with sinusoidal temperature distributions on both sidewalls. *Numer. Heat Transf. A* **2011**, *59*, 167–184. [CrossRef]

20. Li, Q.; Wang, J.; Wang, J.; Baleta, J.; Min, C.; Sundén, B. Effects of gravity and variable thermal properties on nanofluid convective heat transfer using connected and unconnected walls. *Energy Convers. Manag.* **2018**, *171*, 1440–1448. [CrossRef]

21. Bhardwaj, S.; Dalal, A.; Pati, S. Influence of wavy wall and non-uniform heating on natural convection heat transfer and entropy generation inside porous complex enclosure. *Energy* **2015**, *79*, 467–481. [CrossRef]

22. Sivasankaran, S.; Cheong, H.T.; Bhuvaneswari, M.; Ganesan, P. Effect of moving wall direction on mixed convection in an inclined lid-driven square cavity with sinusoidal heating. *Numer. Heat Transf. A* **2016**, *69*, 630–642. [CrossRef]

23. Cheong, H.T.; Siri, Z.; Sivasankaran, S. Effect of aspect ratio on natural convection in an inclined rectangular enclosure with sinusoidal boundary condition. *Int. Comm. Heat Mass Transf.* **2013**, *45*, 75–85. [CrossRef]

24. Sivakumar, V.; Sivasankaran, S. Mixed convection in an inclined lid-driven cavity with non-uniform heating on both sidewalls. *J. Appl. Mech. Tech. Phy.* **2014**, *55*, 634–649. [CrossRef]

25. Hadidi, N.; Bennacer, R.; Ould-amer, Y. Two-dimensional thermosolutal natural convective heat and mass transfer in a bi-layered and inclined porous enclosure. *Energy* **2015**, *93*, 2582–2592. [CrossRef]

26. Wang, H.; Chen, J.; Dai, P.; Zhang, F.; Li, Q. Simulation and Experimental Study of the Influence of the Baffles on Solar Chimney Power Plant System. *Processes* **2021**, *9*, 902. [CrossRef]

27. Thao, P.B.; Truyen, D.C.; Phu, N.M. CFD Analysis and Taguchi-Based Optimization of the Thermohydraulic Performance of a Solar Air Heater Duct Baffled on a Back Plate. *Appl. Sci.* **2021**, *11*, 4645. [CrossRef]

28. Alazwari, M.A.; Safaei, M.R. Combination Effect of Baffle Arrangement and Hybrid Nanofluid on Thermal Performance of a Shell and Tube Heat Exchanger Using 3-D Homogeneous Mixture Model. *Mathematics* **2021**, *9*, 881. [CrossRef]

29. Yu, L.; Xue, M.; Zhu, A. Numerical Investigation of Sloshing in Rectangular Tank with Permeable Baffle. *J. Mar. Sci. Eng.* **2020**, *8*, 671. [CrossRef]

30. Mahapatra, S.K.; Sarkar, A. Numerical simulation of opposing mixed convection in differentially heated square enclosure with partition. *Int. J. Therm. Sci.* **2007**, *46*, 970–979. [CrossRef]

31. Ilis, G.G.; Mobedi, M.; Oztop, H.F. Heat transfer reduction due to a ceiling-mounted barrier in an enclosure with natural convection. *Heat Transf. Eng.* **2011**, *32*, 429–438. [CrossRef]

32. Khatamifar, M.; Lin, W.; Armfield, S.W.; Holmes, D.; Kirkpatrick, M.P. Conjugate natural convection heat transfer in a partitioned differentially-heated square cavity. *Int. Comm. Heat Mass Transf.* **2017**, *81*, 92–103. [CrossRef]